55th 3AF International Conference on Applied Aerodynamics
23 – 25 March 2020, Poitiers - France

A coupled LDVM / IBM investigation of incompressible flows around moving profiles at low Reynolds number

Portzer J.B.[1,2], Faure T.M.[2], Montagnier O.[2] and Serre E.[1]

1 Aix-Marseille Université, CNRS, Centrale Marseille, M2P2 Marseille, France
2 Centre de Recherche de l'École de l'Air, École de l'Air, B.A. 701, 13661 Salon-de-Provence, France,

ABSTRACT

A numerical solver based on the immersed boundary method has been recently developed on OpenFoam [3], a free software.

In this study, we investigate the Immersed Boundary Method (IBM) at low Reynolds number (*Re*=1000) for incompressible flow around NACA 0012 airfoil and then around a flat plate and a NACA 23012 airfoil in rotation (from 0° to 90°). The Leading-edge suction parameter Discrete Vortex Method (LDVM) is also investigated in the models using a rotation of the airfoils.

LIST OF SYMBOLS

c	Chord length
C_L	Lift coefficient
C_D	Drag coefficient
n	Time step
p	Pressure
R_e	Reynolds number
t	Time
u	Flow velocity
$\hat{u}$	Estimated velocity during the predictor step
U_∞	Input velocity

1. INTRODUCTION

Deep stall is a specific dangerous form of airplane stall. It occurs when there is a stall on the main wing and the horizontal tail is inside the detached wake of the main wing. The tail loses its efficiency, leading to a stable pitching equilibrium without any easy recovery method. This phenomenon affects certain aircraft designs, most notably those with a T-tail configuration. It is so of primary importance to investigate in details the flow features as well as the physical mechanisms leading to this phenomenon in order to develop efficient control strategies as well as reliable predictions methods during the conceptual and preliminary design phase of T-tail aircraft.

In this study, we aimed at investigating the flow developing over two-NACA 23 012-airfoils as proposed in Hétru (2015) using a high-fidelity model of DNS implemented in OpenFOAM and based on a recent and efficient Immersed Boundary Method [3]. The IBMpisoFoam solver was validated with a cylinder geometry [3] and for thin airfoils [13] at low Reynolds numbers (*Re*<200). However, some preliminary tests show that the mass error (Eq14) seems to increase with the value of the Reynolds numbers. For a first validation, simulation for thin airfoil profile at higher Reynolds (*Re*=1000) is necessary.

The validation of the method carried out for flows over bluff bodies [3] is extended here for flows over airfoils at low Reynolds number (*Re* = 1000) and at low angle of attack (0° and 10°) [10]. The flow over a moving flat plate with a rotation from 0° to 90° is then considered. The Lagrangian mesh used to model the airfoil in the Immersed Boundary Method is adapted here to avoid mass leakage when moving over the Eulerian fixed mesh where fluid equations are resolved [13]. Despite spurious high frequencies oscillations due to the spatial uncertainty of the moving solid frontier, the aerodynamics coefficients of drag and lift are accurately recovered with respect to the literature. In addition, a Leading-edge-suction-parameter modulated Discrete Vortex Method [12] is calibrated from the DNS to be used as a reduced model in future investigations.

2. RESEARCH METHOD

2.1. Immersed Boundary method (IBM)

The incompressible flow is described by the unsteady and dimensionless Navier-Stockes equations:

$$\nabla . u = 0 \tag{1}$$

$$\frac{\partial u}{\partial t} + \nabla . (uu) = -\nabla p + \frac{1}{R_e}\Delta u \tag{2}$$

The geometry is defined by the use of Lagrangian points in the Eulerian mesh (Fig.1). A penalization method is used to impose a non slip condition in the cells where the Lagrangian markers are located.

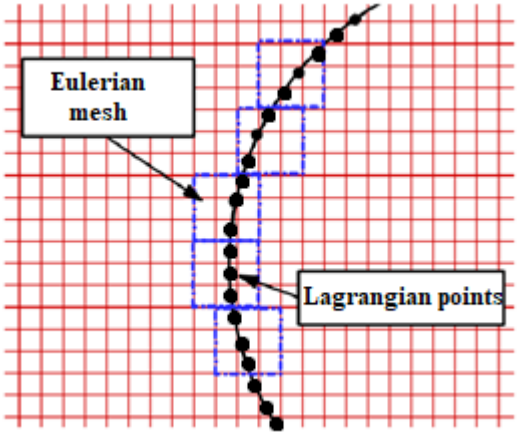

Figure 1: Definition of the geometry

The predictor-corrector solver pisoFOAM (used in body-fitted method) has been modified [3] to inclined the definition of a force term f (Fig.2).

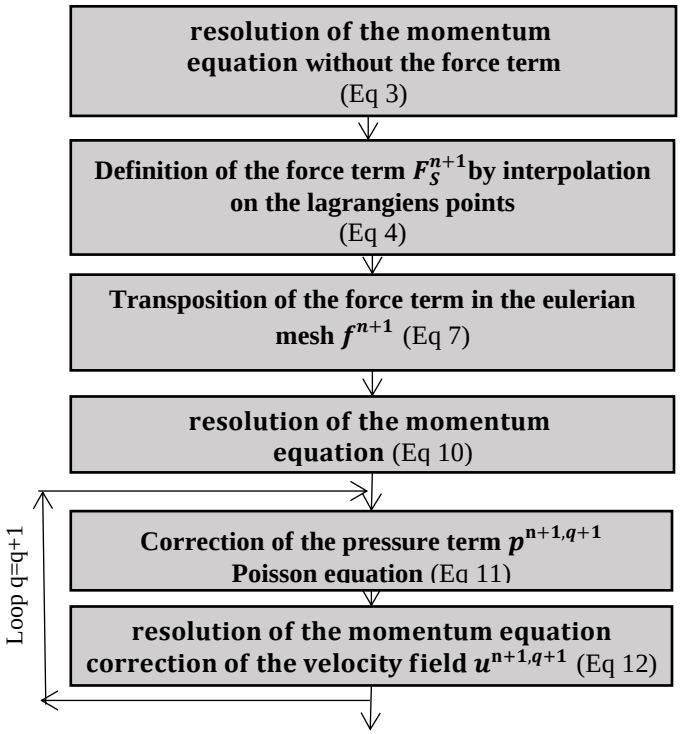

Figure 2: IBMpisoFOAM solver at each time step (n+1)

$$\frac{\partial \hat{u}}{\partial t} + \nabla.(\hat{u}\hat{u}) = -\nabla p + \frac{1}{R_e}\Delta\hat{u} \quad (3)$$

$$F_S^{n+1} = \frac{U_S^d - I[\hat{u}]_S}{\Delta t} \quad (4)$$

With U_s^d the target velocity and $I[\hat{u}]_s$the interpolation of the fluid velocity at the Lagrangian marker s.

$$I[\hat{u}]_S = \sum_{j\in D_S} u_j^n \delta_h(x_j - X_s)\Delta v \quad (5)$$

x_j is the position of the centre of the cell *j*, X_s is the position of the Lagrangian marker *s* and Δv refers to the Eulerian quadrature ($\Delta v = \Delta x \Delta y \Delta z$) for the case of a Cartesian uniform mesh δ_h is the discretized delta function used in [14].

$$\delta_h = \begin{cases} \frac{1}{3}\left(1+\sqrt{-3r^2+1}\right) & 0 \le r \le 0.5 \\ \frac{1}{6}\left(5-3r-\sqrt{-3(1-r)^2+1}\right) & 0.5 \le r \le 1.5 \\ 0 & 1.5 < r \end{cases} \quad (6)$$

$$f^{n+1}(x_j) = \sum_{j\in D_S} F_S^{n+1}\delta_h(x_j - X_k)\varepsilon_k \quad (7)$$

The *k*-index refers to a loop over the lagrangian markers whose support contains the Eulerian node *j*. ε_k is the Lagrangian quadrature, which is calculated by solving a linear system:

$$A\varepsilon = 1 \quad (8)$$

Where the vectors $\varepsilon = (\varepsilon_1, \dots, \varepsilon_{Ns})^T$ and $1 = (1, \dots, 1)^T$ have a dimension *Ns* corresponding to the number of lagrangian markers. *A* is the matrix defined by the product between the $k^{th}$and the m^{th} interpolation kernels such that:

$$A_{km} = \sum_{j\in D_m} \delta_h(x_j - X_k)\delta_h(x_j - X_m) \quad (9)$$

$$\frac{\partial u^{*,1}}{\partial t} + \nabla.(u^{n+1,1}u^{n+1,1}) = -\nabla p + \frac{1}{R_e}\Delta u^{n+1,1} + f(\hat{u}) \quad (10)$$

$$\nabla^2 p^{n+1,q+1} = -\nabla.(u^{n+1,q}\nabla u^{n+1,q}) + \nabla.f(\hat{u}) \quad (11)$$

$$\frac{\partial u^{n+1,q+1}}{\partial t} + \nabla.(u^{n+1,q+1}u^{n+1,q+1}) = -\nabla p^{n+1,q+1} + \frac{1}{R_e}\Delta u^{n+1,q+1} + f(\hat{u}) \quad (12)$$

2.2. Correction of the force term

The main problem with a penalization method in IBM is the precision in the non-slipping condition. In fact, for the incompressible case, the force term is not corrected during the correction loop. This error can be estimated with me maximum residual velocity value (*Vres)* or the error mass value.

$$V_{res} = \max(u_k)/U_\infty \quad (13)$$

$$error\ mass = \max(\rho_{ij} div(u_{ij}) S_{ij}) \quad (14)$$

With S_{ij} the area of the cell (*i*,*j*) and u_k the value of the residual velocity at the k^{th} lagrangian marker.

Following a suggestion [13] used for the compressible IBM solver, a correction of the force term is also tested (Eq. 15).

$$F_s^{n+1} = \frac{U_s^d - I[\hat{u}]_s}{\Delta t} + grad(p) \qquad (15)$$

2.3. Mesh

The present study performs simulations at *Re*=1000, the flow is laminar, therefore a large domain is needed (Fig.3). The structured grid is used and since this is a DNS simulation, the cell size shall be dx=dy=1/*Re*=0.001c near the geometry (Fig. 4,5,6).

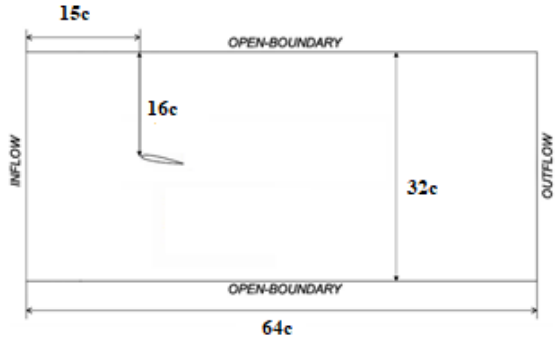

Figure 3: Numerical domain

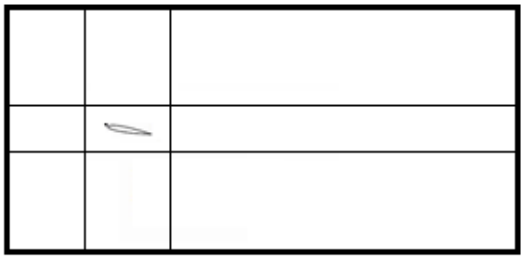

Figure 4: Mesh used in IBM simulations (different regions)

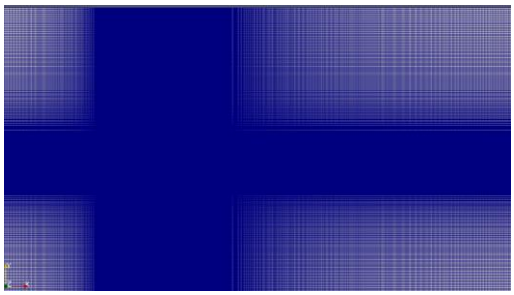

Figure 5: Structured mesh used in IBM simulations

In order to compare the IBM with the classical CFD approach, a C-shaped body-fitted structured mesh is used with the non-modified pisoFoam solver. (The predictor is defined by Eq3 and the corrector loop with Eq11 and Eq12 in which $f(\hat{u})$ is null).

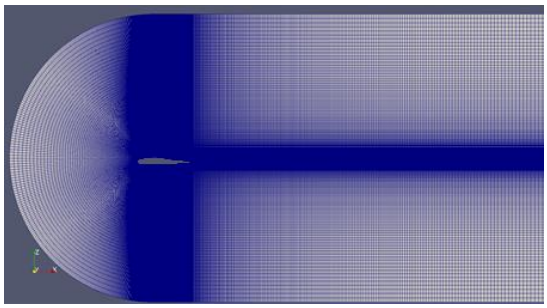

Figure 6: Body fitted mesh

2.4. LDVM method

The Leading edge suction parameter Discrete Vortex Method (LDVM) is based on the potential thin airfoil theory in unsteady flows, applicable for large values of the angle of attack [12]. It is built on the time-stepping approach of [9] with the addition of a criterion for the leading edge detachment.

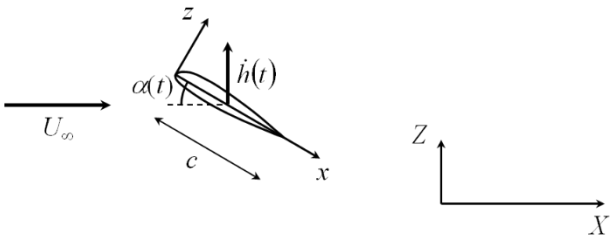

Figure 7. Airfoil motion and frames of reference.

In Fig.7, the aerodynamic frame (*X*,*Z*) is fixed and the airfoil frame (*x*,*z*) sees an upstream velocity U_∞ aligned on the *X* axis with a time-dependant angle of attack $\alpha(t)$. A vertical motion $h(t)$ is considered along the *Z* axis. The fluid velocity components are respectively *U* and *W* in the aerodynamic frame and *w* is the velocity along *z* in the airfoil frame. The local circulation distribution over the airfoil is obtained from a Fourier series:

$$\gamma(\theta,t) = 2U_\infty \left[A_0(t)\frac{1+\cos\theta}{\sin\theta} + \sum_{n=1}^{\infty} A_n(t)\sin n\theta \right] \qquad (16)$$

with $A_0(t)$, … , $A_n(t)$ the time-dependant Fourier coefficients, *c* the airfoil chord and with:

$$x = \frac{c}{2}(1-\cos\theta) \qquad (17)$$

The Kutta condition is enforced through the form of the Fourier series. The Fourier coefficients are determined from the instantaneous local downwash $w(\theta,t)$ by enforcing the potential flow boundary condition that the velocity is tangential to the airfoil surface:

$$A_0(t) = -\frac{1}{\pi}\int_0^\pi \frac{w(\theta,t)}{U_\infty} d\theta \qquad (18)$$

$$A_n(t) = \frac{2}{\pi}\int_0^\pi \frac{w(\theta,t)}{U_\infty} \cos n\theta \, d\theta \qquad (19)$$

where $w(\theta,t)$ is the velocity normal to the airfoil calculated from the motion kinematics:

$$\begin{aligned} w(\theta,t) = & \frac{\partial \eta}{\partial x}\left(U_\infty \cos\alpha + \dot{h}\sin\alpha + \frac{\partial \Phi_{TEV}}{\partial x} + \frac{\partial \Phi_{LEV}}{\partial x} \right) \\ & - U_\infty \sin\alpha - \dot{\alpha}\left(x - x_p\right) - \dot{h}\cos\alpha \\ & - \frac{\partial \Phi_{TEV}}{\partial x} - \frac{\partial \Phi_{LEV}}{\partial x} \end{aligned} \tag{20}$$

with Φ_{TEV}, Φ_{LEV} the velocity potentials associated with the leading edge and trailing edge vortices, η the airfoil mean camber line and x_p the pivot position. At each time step, if the flow around the airfoil is attached, a trailing edge vortex (TEV) is released and advected by the flow at the following time step. However, a separation model is needed for large values of the angle of attack. The separation on the airfoil is obtained with an inviscid parameter developed by [12]. The Leading Edge Suction Parameter (LESP) is a non-dimensional measure of the suction at the leading edge, and equates the first Fourier coefficient:

$$\mathrm{LESP}(t) = A_0(t) \tag{21}$$

The critical value LESP_{crit} corresponds to the A_0 value associated with the angle of attack for which spikes appear in the negative part of the friction coefficient, near the leading edge. It is a measure of the maximum suction that a given airfoil can bear before separation and is independent of the motion. Beyond that LESP_{crit} value, the airfoil suction side boundary layer separates from the leading edge, which corresponds to the release of a leading edge vortex (LEV). In that case, there is shedding of both a TEV and a LEV. These vortices, at every time step, must enforce Kelvin's circulation theorem:

$$\Gamma_B(t) + \sum_{k=1}^{i} \Gamma_{TEV,k} + \sum_{l=1}^{i} \Gamma_{LEV,l} = 0 \tag{22}$$

with the airfoil bound circulation:

$$\Gamma_B(t) = \int_0^\pi \gamma(\theta,t)\,d\theta = U_\infty c\pi\left[A_0(t) + \frac{A_1(t)}{2} \right] \tag{23}$$

The previous variables are written in a non-dimensional form for the fluid mechanics problem as:

$$\begin{aligned} w^* &= \frac{w}{U_\infty} \quad U^* = \frac{w}{U_\infty} \quad W^* = \frac{W}{U_\infty} \\ X^* &= \frac{X}{c} \quad Z^* = \frac{Z}{c} \quad \Gamma^* = \frac{\Gamma}{U_\infty c} \end{aligned} \tag{24}$$

The velocity induced by a given vortex is described with the model of Vatistas which incorporates a finite core radius r_c [17].

$$\begin{aligned} U_k^* &= \frac{\Gamma_k^*}{2\pi} \frac{Z^* - Z_k^*}{\sqrt{\left[\left(X^* - X_k^*\right)^2 + \left(Z^* - Z_k^*\right)^2 \right]^2 + r_c^{*4}}} \\ W_k^* &= -\frac{\Gamma_k^*}{2\pi} \frac{X^* - X_k^*}{\sqrt{\left[\left(X^* - X_k^*\right)^2 + \left(Z^* - Z_k^*\right)^2 \right]^2 + r_c^{*4}}} \end{aligned} \tag{25}$$

The non-dimensional time step is:

$$\delta t^* = \frac{\delta t U_\infty}{c} = 0.015 \tag{26}$$

The vortex core radius is taken to be 1.3 times the average spacing between the vortices [5]:

$$r_c^* = \frac{r_c}{c} = 1.3\delta t^* \tag{27}$$

The last shed vortex is placed at one third of the distance from the shedding edge to the previously shed vortex [9]:

$$\begin{aligned} X_{TEV,k}^* &= X_{TE}^* + \frac{1}{3}\left(X_{TEV,k-1}^* - X_{TE}^* \right) \\ Z_{TEV,k}^* &= Z_{TE}^* + \frac{1}{3}\left(Z_{TEV,k-1}^* - Z_{TE}^* \right) \\ X_{LEV,l}^* &= X_{LE}^* + \frac{1}{3}\left(X_{LEV,l-1}^* - X_{LE}^* \right) \\ Z_{LEV,l}^* &= Z_{LE}^* + \frac{1}{3}\left(Z_{LEV,l-1}^* - Z_{LE}^* \right) \end{aligned} \tag{28}$$

For each time-step, the unknown parameters are the circulations corresponding to the newly shed vortices, advected by the velocity field. Firstly, if there is only a TEV shed at the iteration i, equation (20) is reduced to:

$$w^*\left(\theta, t_i^*\right) = T_1 + \Gamma_{TEV,i}^* T_2 \tag{29}$$

where T_1 and T_2 are terms depending on the angle of attack, the vertical displacement and the summation of the influence of the previously shed vortices. The only unknown parameter is the circulation of the TEV shed at iteration i. The airfoil bound circulation is obtained from (8) substituting the Fourier coefficients:

$$\begin{aligned} \Gamma_B^* &= \int_0^\pi T_1\left(\cos\theta - 1\right)d\theta + \Gamma_{TEV,i}^* \int_0^\pi T_2\left(\cos\theta - 1\right)d\theta \\ &= I_1 + I_2 \Gamma_{TEV,i}^* \end{aligned} \tag{30}$$

where I_1 and I_2 are terms resulting of the integrals of T_1 and T_2. Substituting (15) into Kelvin's theorem (22):

$$\Gamma_{TEV,i}^* = -\frac{I_1 + \sum_{k=1}^{i-1} \Gamma_{TEV,k}^* + \sum_{l=1}^{i-1} \Gamma_{TEV,l}^*}{1 + I_2} \tag{31}$$

Secondly, if both a TEV and LEV are shed at iteration i, then equation (5) is reduced to:

$$w^*\left(\theta, t_i^*\right) = T_1 + \Gamma_{TEV,i}^* T_2 + \Gamma_{LEV,i}^* T_3 \tag{32}$$

where T_1, T_2 and T_3 are terms depending on the angle of attack, the vertical displacement and the summation of the influence of the previously shed vortices. There is two unknown parameters which are the circulations of the TEV and LEV shed at iteration i, requiring two equations. The airfoil bound circulation is obtained from (8) substituting the Fourier coefficients:

$$\Gamma_B^* = I_1 + I_2 \Gamma_{TEV,i}^* + I_3 \Gamma_{LEV,i}^* \tag{33}$$

where I_1, I_2 and I_3 are terms resulting of the integrals of T_1, T_2 and T_3. Kelvin's theorem (22) and the criterion on the critical LESP provide:

$$\Gamma_B^* + \Gamma_{TEV,i}^* + \Gamma_{LEV,i}^* + \sum_{k=1}^{i-1}\Gamma_{TEV,k}^* + \sum_{l=1}^{i-1}\Gamma_{LEV,l}^* = 0$$
$$A_0 - \mathrm{LESP}_{crit} = 0 \tag{34}$$

Substituting the bound circulation and the value of A_0, equation (19) is:

$$I_1 + \Gamma_{TEV,i}^*(1+I_2) + \Gamma_{LEV,i}^*(1+I_3) + \sum_{k=1}^{i-1}\Gamma_{TEV,k}^* + \sum_{l=1}^{i-1}\Gamma_{LEV,l}^* = 0$$
$$J_1 + J_2\Gamma_{TEV,i}^* + J_3\Gamma_{LEV,i}^* - \mathrm{LESP}_{crit} = 0 \tag{35}$$

Note that this is a linear system, and no iteration scheme is required as previously mentioned in [12] and [9]. Therefore, a significant gain in calculation time is expected [6]. As only the shed LEV and TEV are computed with the method, it is worth noticing that the simulation time is increasing with the number of vortices. In order to reduce that number, the vortices located four chords downstream of the leading edge can be amalgamated into larger structures [16]. That clustering can be realized with a multidimensional binary search tree or *k*-d tree [2], for all the vortices downstream of four chords of the airfoil.

The unsteady form of the Bernoulli theorem is used to calculate the pressure distribution along the airfoil:

$$p_{ps} - p_{ss} = \rho\left[\frac{1}{2}\left(V_{t,ss}^2 - V_{t,ps}^2\right) + \frac{\partial\Phi_{ss}}{\partial t} - \frac{\partial\Phi_{ps}}{\partial t}\right] \tag{36}$$

with the indices *ps* and *ss* respectively for the pressure side and suction side and V_t the tangential velocity. As the flow potential function is the sum of the potential functions of the bound circulation, TEV and LEV:

$$\Phi = \Phi_B + \Phi_{TEV} + \Phi_{LEV} \tag{37}$$

the tangential velocity is:

$$V_{t,ss} = U_\infty\cos\alpha + \dot{h}\sin\alpha + \left(\frac{\partial\Phi_B}{\partial x}\right)_{ss} + \left(\frac{\partial\Phi_{TEV}}{\partial x}\right)_{ss} + \left(\frac{\partial\Phi_{LEV}}{\partial x}\right)_{ss} \tag{38}$$

$$V_{t,ps} = U_\infty\cos\alpha + \dot{h}\sin\alpha + \left(\frac{\partial\Phi_B}{\partial x}\right)_{ps} + \left(\frac{\partial\Phi_{TEV}}{\partial x}\right)_{ps} + \left(\frac{\partial\Phi_{LEV}}{\partial x}\right)_{ps} \tag{39}$$

From the thin airfoil theory:

$$\left(\frac{\partial\Phi_B}{\partial x}\right)_{ss} = \frac{\gamma(x,t)}{2} \qquad \left(\frac{\partial\Phi_B}{\partial x}\right)_{ps} = -\frac{\gamma(x,t)}{2} \tag{40}$$

Then:

$$V_{t,ss}^2 - V_{t,ps}^2 = 2\left[U_\infty\cos\alpha + \dot{h}\sin\alpha + \frac{\partial\Phi_{TEV}}{\partial x} + \frac{\partial\Phi_{LEV}}{\partial x}\right]\gamma(x,t) \tag{41}$$

The potential functions time derivatives are:

$$\frac{\partial\Phi_{ss}}{\partial t} - \frac{\partial\Phi_{ps}}{\partial t} = \frac{\partial}{\partial t}\int_0^x\gamma(\xi,t)d\xi \tag{42}$$

Hence (21) becomes:

$$p_{ps} - p_{ss} = \rho\left\{\left[U_\infty\cos\alpha + \dot{h}\sin\alpha + \frac{\partial\Phi_{TEV}}{\partial x} + \frac{\partial\Phi_{LEV}}{\partial x}\right]\gamma(x) + \frac{\partial}{\partial t}\int_0^x\gamma(\xi,t)d\xi\right\} \tag{43}$$

The normal force on the airfoil is obtained:

$$F_N = \rho\left[\int_0^c\left(U_\infty\cos\alpha + \dot{h}\sin\alpha + \frac{\partial\Phi_{TEV}}{\partial x} + \frac{\partial\Phi_{LEV}}{\partial x}\right)\gamma(x,t)d\xi + \int_0^c\frac{\partial}{\partial t}\int_0^x\gamma(\xi,t)d\xi dx\right] \tag{44}$$

Using the Fourier coefficients, it is reduced to:

$$F_N = \rho U_\infty c\pi\left[\left(U_\infty\cos\alpha + \dot{h}\sin\alpha\right)\left(A_0 + \frac{A_1}{2}\right) + c\left(\frac{3\dot{A}_0}{4} + \frac{\dot{A}_1}{4} + \frac{\dot{A}_2}{8}\right) + \rho\int_0^c\left(\frac{\partial\Phi_{TEV}}{\partial x} + \frac{\partial\Phi_{LEV}}{\partial x}\right)\gamma(x,t)dx\right] \tag{45}$$

The axial force is given by the Blasius formula [9]:

$$F_A = \rho U_\infty^2 c\pi A_0^2 \tag{46}$$

Similarly, the moment about the position x_{ref} on the airfoil is:

$$M = x_{ref}F_N - \rho U_\infty c^2\pi\left[\left(U_\infty\cos\alpha + \dot{h}\sin\alpha\right)\left(\frac{A_0}{4} + \frac{A_1}{4} - \frac{A_2}{8}\right) + c\left(\frac{7\dot{A}_0}{16} + \frac{3\dot{A}_1}{16} + \frac{\dot{A}_2}{16} - \frac{\dot{A}_3}{64}\right) - \rho\int_0^c\left(\frac{\partial\Phi_{TEV}}{\partial x} + \frac{\partial\Phi_{LEV}}{\partial x}\right)\gamma(x,t)xdx\right] \tag{47}$$

3. RESULTS

3.1. Validation of the model

The Immersed boundary method is compared with the body-fitted method and the numerical simulations from Kurtulus [10] for 2D NACA 0012 wings at 0° and 10° (Fig.8).

As expected (Tab.1), the simulations with the body-fitted method (pisoFoam solver) correspond to the other CFD models (1% error for C_D and C_L) [10] and despite a one order of magnitude higher of difference for the error mass between the IBM solver and the body-fitted method, the solver seems quite accurate (11% difference for the value of C_L and 4% difference with the C_D value). (Fig. 9,10)

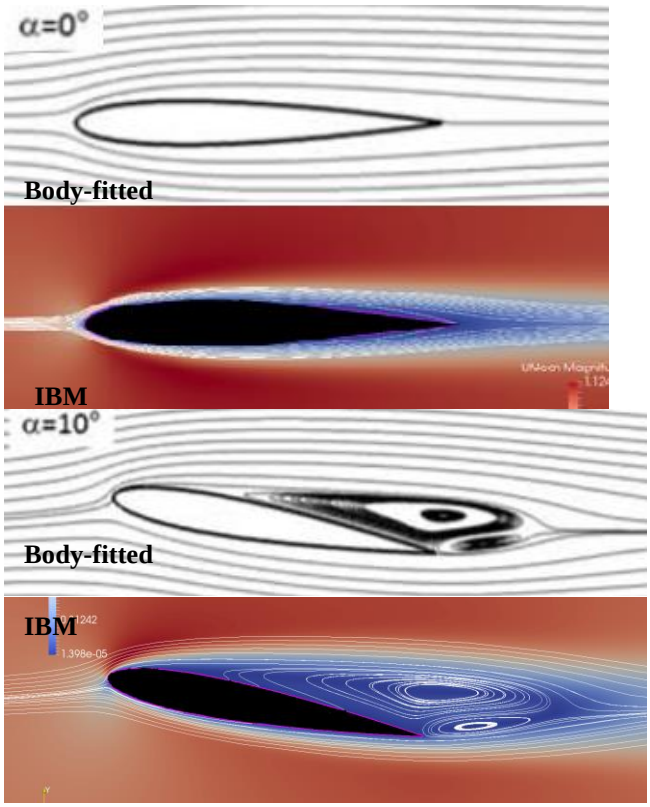

Figure 8: Streamlines of mean velocity field for 0° and 10° angle of attack (NACA0012 *Re*=1000)

Table 1: NACA0012 *Re*=1000 α=10°

	C_L	C_D	Strouhal	C_L/C_D	Error mass	*Vres*
Dilek Funda Kurtulus [10]	0,425	0,165	0,876	2,58		
Body fitted method	0,420	0,164	0,8	2,56	3,5E-06	
IBM	0,479	0,172	0,8	2,78	2,5E-05	2,5%
IBM and correction force term	0,501	0,176	0,7	2,85	2,5E-05	5,4%

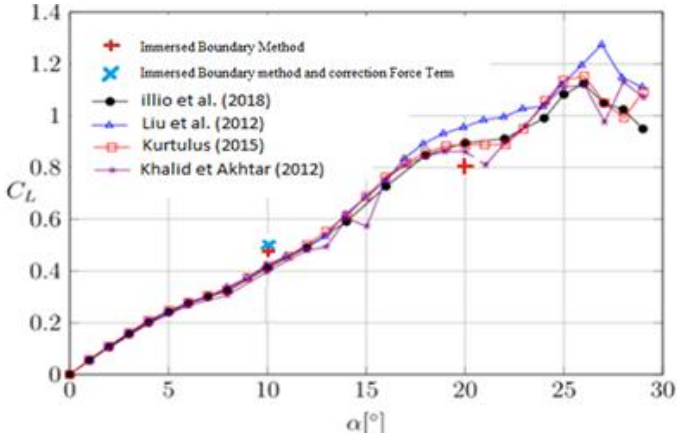

Figure 9: Lift coefficient NACA0012 *Re*=1000

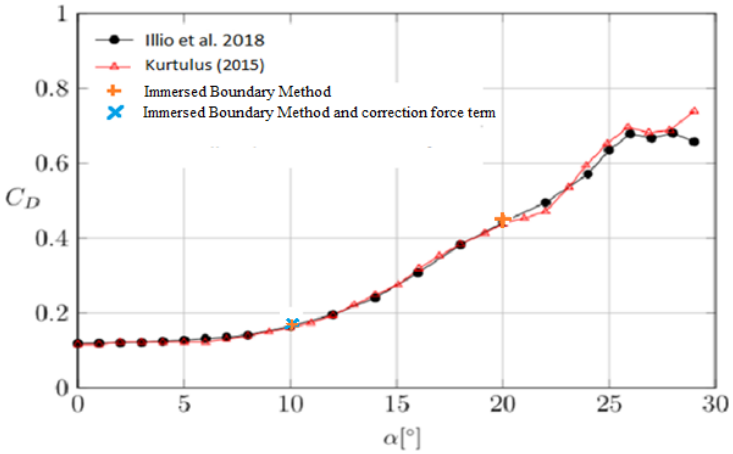

Figure 10: Drag coefficient NACA0012 *Re*=1000

The highest errors on the penalization force term are concentrated at the leading edge. In fact, the maximum residual velocity is at this location and his value is approximately five times the mean value of residual velocities.

The correction of the force term with the pressure gradient do not succeed to increase the accuracy of the penalisation method but increase the error on the residual velocity value.

A high correlation seems to exist (R^2>0.95) between the value of *Vres* and the error obtained for the C_D and C_L value (considering to the body-fitted method as a reference).

3.2. Computation of rotational movement of a flat plate

Following the objective of studying the deep stall phenomenon, the displacement of airfoils must be implemented and validated for the solver. In this study, we use the rotation of a flat plate from 0° to 90° angle as described in the case 5A in Ramesh (2014) [12].

The function of the movement is smoothed [4] [12] to avoid a virtual mass phenomenon.

$$G(t) = ln\left[\frac{\cosh(a(t-t_1))\cosh(a(t-t_4))}{\cosh(a(t-t_2))\cosh(a(t-t_3))}\right] \quad (41)$$

$$K = 0.2; a = 11;\ t_1 = 1;\ t_2 = t_1 + \frac{Am}{2K} \quad (42)$$

$$t_3 = t_2 + \frac{\pi \times Am}{4K} - \frac{Am}{2K};\ t_4 = t_3 + \frac{Am}{2K}; \quad (43)$$

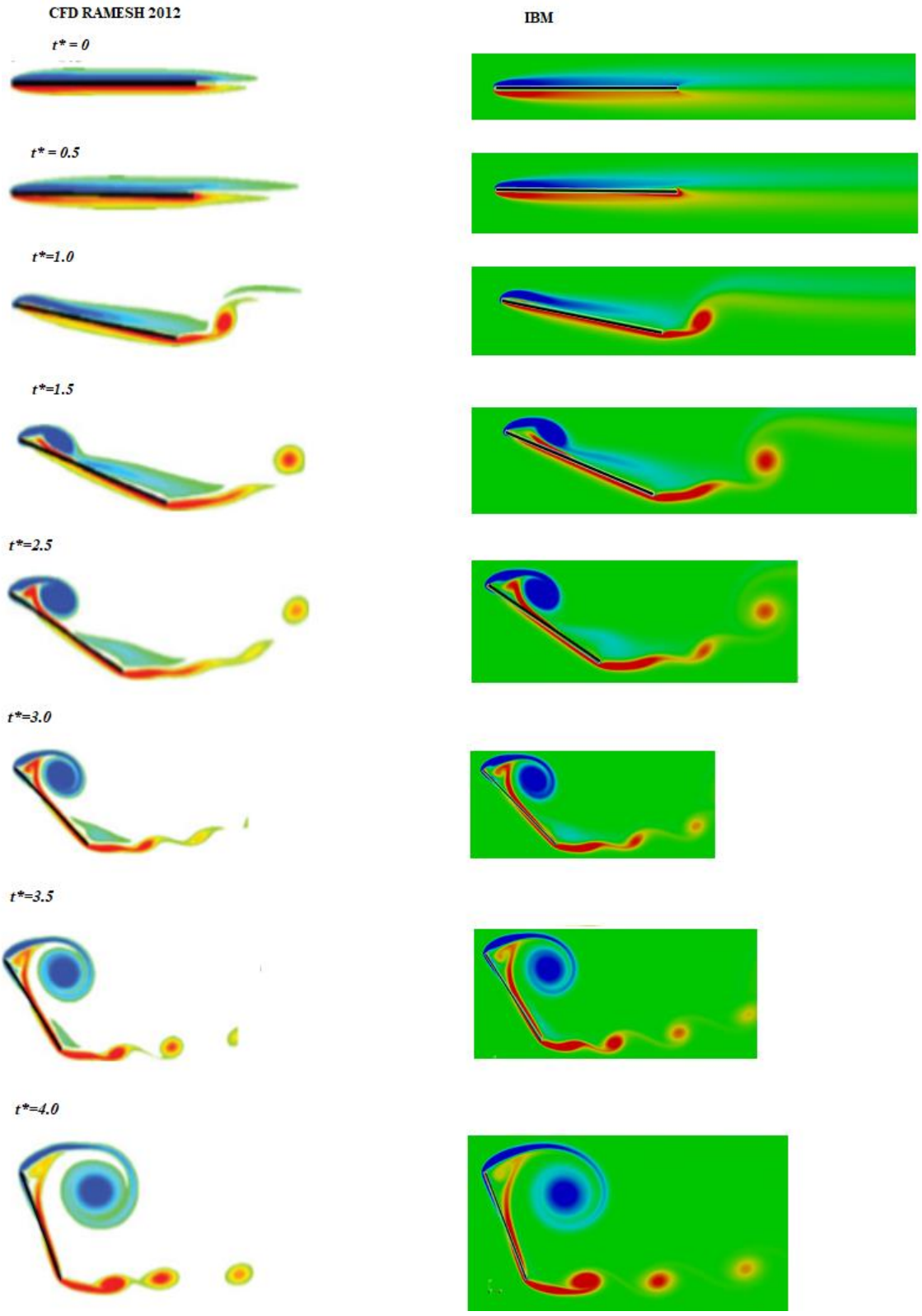

Figure 11: Flat plate in rotation (*Re*=1000). Comparison of flow features between IBM and CFD of Wang & Eldredge (2013) for t^* from 0.5 to 4.0.

$$\alpha(t) = \frac{G(t)\times Am}{\max\,(G(t))} \quad \text{with} \quad Am = \frac{\pi}{2} \qquad (44)$$

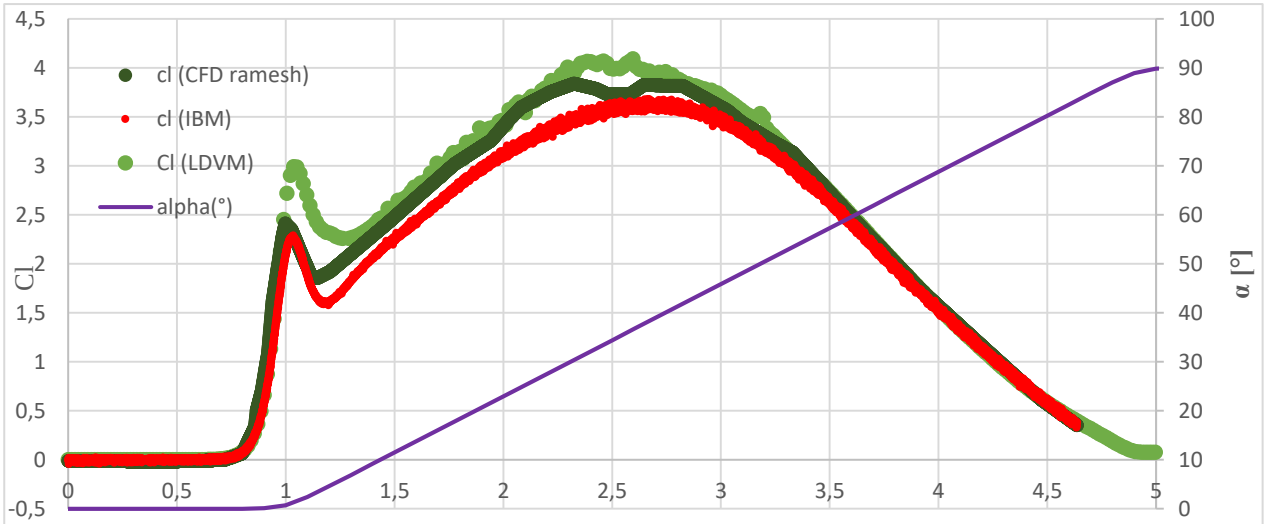

Figure 12: Drag coefficient of a flat plate in rotation (Re=1000) and comparison with Ramesh (2014) [9]

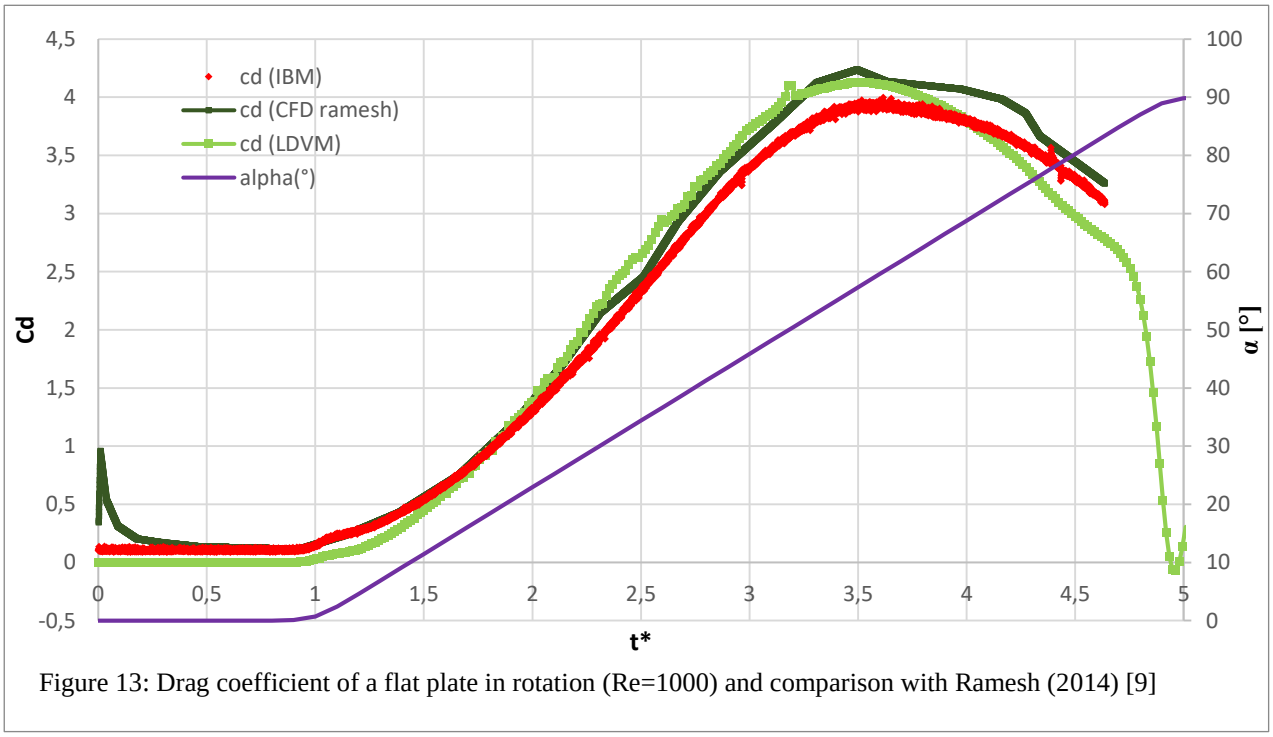

Figure 13: Drag coefficient of a flat plate in rotation (Re=1000) and comparison with Ramesh (2014) [9]

With *Am* the maximum value of angle $\left(\frac{\pi}{2}\right)$. (Fig.12)

A high frequency oscillation can be observed during the movement on the lift and drag coefficient value. This perturbation is due to the change of state of the cells when the Lagrangian markers move. Moreover, even if a time step of $dt = 5 \times 10^{-4}$ is sufficient to keep the courant number < 1, the lift and drag coefficient became independent of the value of the time step for $dt \leq 5 \times 10^{-5}$.

The values of lift and drag coefficient obtained from the Immersed boundary method follows the one obtained from other CFD method [9] (with a relative difference <10%). (Fig. 12,13).

3.3. Computation of a NACA 23012 rotation motion

The next step of this study is to apply a rotation motion on an airfoil. The same rotation is applied on a NACA23012 airfoil (incompressible flow, *Re*=1000).

The vorticity distribution around the airfoil is used [15] to define the angle corresponding to the leading-edge separation which is 21.4°. This allow to define a $LESP_{crit}$ =0.3. (Fig.14)

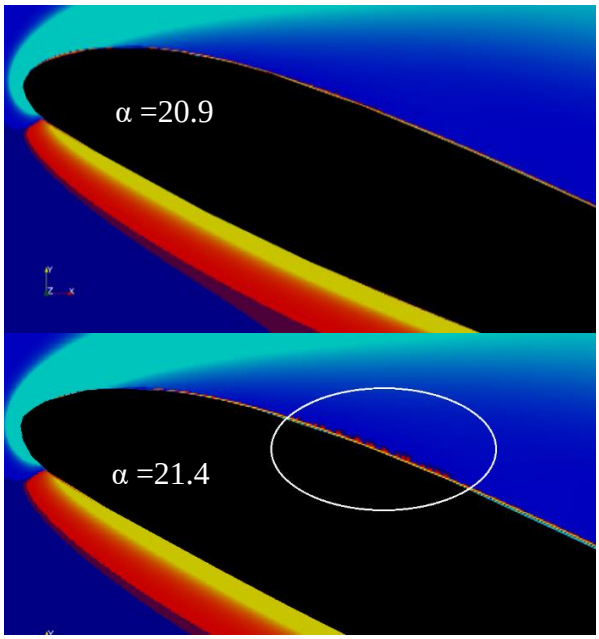

Figure 14: Vorticity around a NACA23012 airfoil in rotation (Re=1000). Start of the leading-edge separation.

However, there is a great disparity in the lift and drag coefficient between the IBM and the LDVM. The gap between the values of C_L is twice the one observed for the flat plane (Fig 16).

This result is due to the geometry of the NACA23012. In fact, this geometry is out of the domain of validity of the LDVM method: in one hand, the LEV does not appear at the exact position of the leading edge, and in other hand a detached flow occurs on the trailing edge at low angles (α<10°) (Fig 15). None of these phenomena are included in the LDVM solver. A modification of the method to determine the exact location of the generated vortex may increase the domain of validity of the LDVM method to thick airfoils.

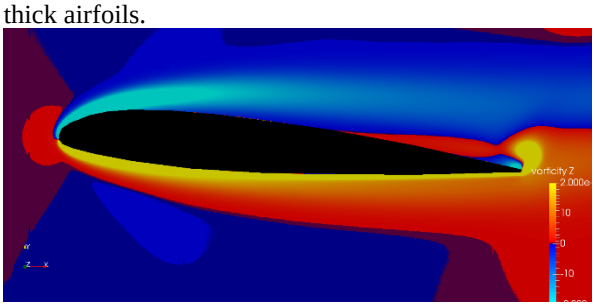
Figure 15: Vorticity around a NACA23012 airfoil in rotation (Re=1000)

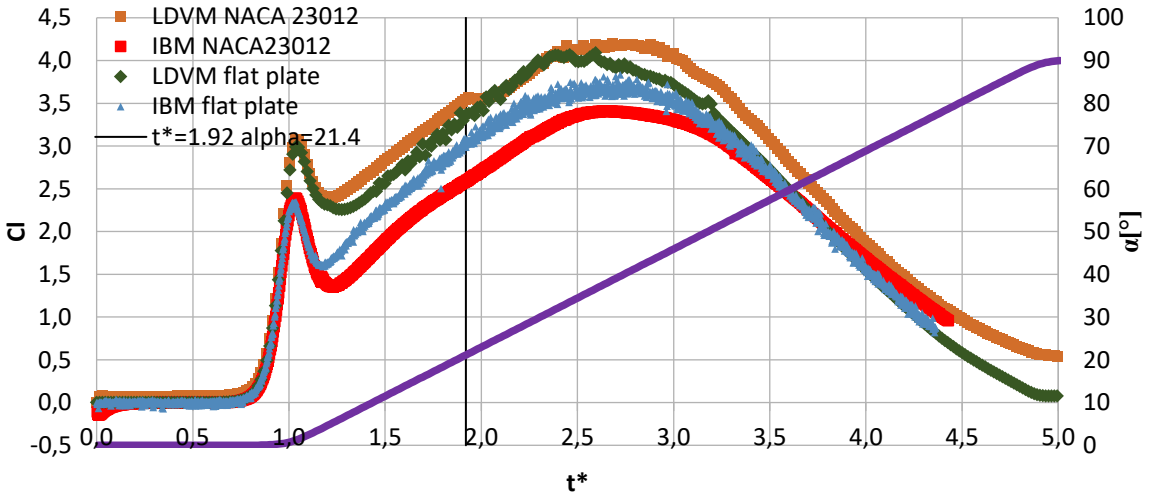

Figure 16: Lift coefficient of an airfoil in rotation (Re=1000)

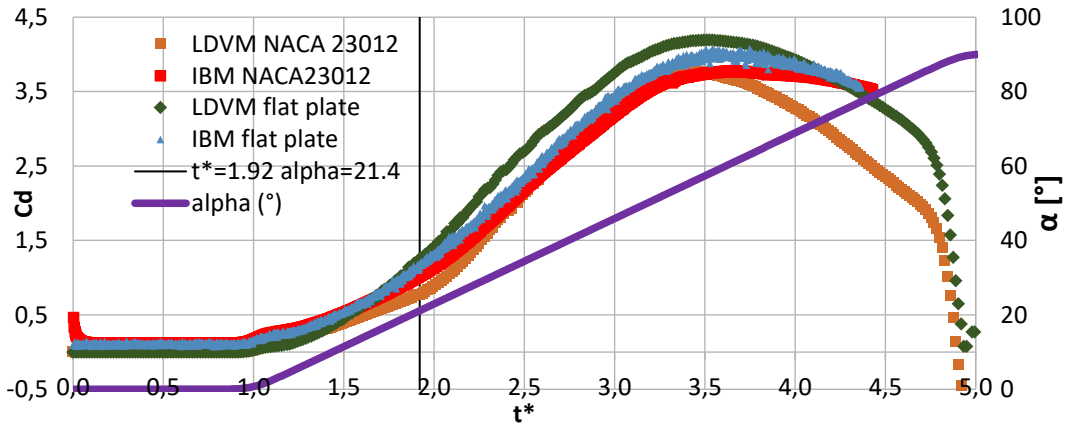

Figure 17: Drag coefficient of an airfoil in rotation (Re=1000)

4. CONCLUSION

The Immersed Boundary incompressible solver developed on OpenFoam is quite accurate for the simulation of flows around airfoils at low Reynolds number (*Re*=1000). The main flaw of the solver is the accuracy of penalization force which directly depends on the time step since the force term is not modified during the correction loop (Eq 11 and Eq12).

The LDVM method actually developed by Ramesh is only adapted for thin airfoils and a way to determine the location of the vortex generated may increase the domain of validity for NACA 23012 airfoil.

That is why the Immersed Boundary Method will be prioritized over the LDVM for our study in vortex forcing resulting from the aerodynamic interaction between two NACA 23012 airfoils.

REFERENCES

1. Ansari, S.A., Żbikowski, R. & Knowles, K. (2006) Nonlinear unsteady aerodynamic
2. Bentley, J.L. (1975) Multidimensional binary search trees used for associative searching, *Communications of the ACM*, 18 (9), 509-517.
3. Constant E., Favier J., Meldi M. & al. (2017) An immersed boundary method in OpenFOAM: verification and validation. *Computers & Fluids*, vol. 157, p. 55-72.
4. Eldredge, J., Wang, C., & Ol, M. (2009, June). A computational study of a canonical pitch-up, pitch-down wing maneuver. In *39th AIAA fluid dynamics conference* (p. 3687).
5. Faure T, Dumas L. Kirsch B.and Montagnier O. (2018) Simulation of the aeroelastic behavior of a possibly detached flow airfoil by a discrete vortex method. *53rd 3AF International Conference.*
6. Faure, T.M., Dumas, L., Drouet, V. & Montagnier, O. (2017) A modified discrete-vortex method with shedding criterion for unsteady or constant angle of attack flow prediction, *Applied Mathematical Modelling*, vol. 69, p. 32-46.
7. Hetru L. (2015) Etude expérimentale et numérique de l'interaction aérodynamique entre deux profils : application au risque aéronautique du décrochage profond. PhD. Aix-Marseille.
8. Issa, R. I. (1986). Solution of the implicitly discretised fluid flow equations by operator-splitting. *Journal of computational physics*, 62(1), 40-65.
9. Katz, J. & Plotkin, A. (2000) *Low-Speed Aerodynamics*, Cambridge University Press
10. Kurtulus, Dilek Funda. On the unsteady behavior of the flow around NACA 0012 airfoil with steady external conditions at Re= 1000. *International Journal of Micro Air Vehicles*, 2015, vol. 7, no 3, p. 301-326.
11. Leonard, A. (1980) Vortex methods for flow simulations, *J. Comput. Phys.* 37 (3), 289-335.
12. Ramesh, Kiran, Gopalarathnam, Ashok, Granlund, Kenneth, *et al.* Discrete-vortex method with novel shedding criterion for unsteady aerofoil flows with intermittent leading-edge vortex shedding. *Journal of Fluid Mechanics*, 2014, vol. 751, p. 500-538.
13. Riahi, H., Meldi, M., Favier, J., *et al.* A pressure-corrected Immersed Boundary Method for the numerical simulation of compressible flows. *Journal of Computational Physics*, 2018, vol. 374, p. 361-383
14. Roma A., Peskin C., Berger M., (1999) An adaptative version of the immersed boundary method. *J Comp Phys*, p509-534
15. Ramesh, K., Ke, J., Gopalarathnam, A., & Edwards, J. (2012, June). Effect of airfoil shape and Reynolds number on leading edge vortex shedding in unsteady flows. In *30th AIAA applied aerodynamics conference* (p. 3025).
16. Sarpkaya, T. (1975) An inviscid model of two-dimensional vortex shedding for transient and asymptotically steady separated flow over an inclined plate, *Journal of Fluid Mechanics* 68 (1), 109-128.
17. Vatistas, G.H., Kozel, V. & Mih, W.C. (1991) A simpler model for concentrated vortices, *Exp. Fluids*, 11 (1), 73-76.